GEODESY AND GEODYNAMICS 2015, VOL 6 NO 1, 41–45

Available online at www.sciencedirect.com

ScienceDirect

journal homepage: www.keaipublishing.com/en/journals/geog; http://www.jgg09.com/jweb_ddcl_en/EN/volumn/home.shtml

Gravity gradient distribution in mainland China from GOCE satellite gravity gradiometry data

Xu Haijun[a,*], *Zhang Yongzhi*[b], *Duan Hurong*[c]

[a] *Institute of Resources and Environment, North China University of Water Resources and Electric Power, Zhengzhou 450011, China*
[b] *College of Geological Engineering and Geomatics, Chang'an University, Xi'an 710054, China*
[c] *College of Geomatics, Xi'an University of Science and Technology, Xi'an 710054, China*

ARTICLE INFO

Article history:
Received 15 October 2014
Accepted 29 December 2014
Available online 23 March 2015

Keywords:
GOCE
Gravity anomaly
Satellite gravity gradiometry
Geological tectonics
Mainland China
Earth's gravity field
Geoid height
Rigorous recursion formula

ABSTRACT

At present, gravity field and steady-state ocean circulation explorer (GOCE) gravity data are always used to compute regional gravity anomaly and geoid height. In this study, the latest GOCE gravity field model data (from Oct. 2009 to Jul. 2010) are used to compute the gravity gradient of mainland China according to a rigorous recursion formula (in all the six directions). The results show that the numerical values of the gravity gradients are larger in the T_{rr} direction than those in the other directions. They reflect the terrain characteristics in detail and correlate with the regional tectonics; however, in the $T_{\theta\lambda}$ and $T_{r\lambda}$ directions, the numerical values are relatively smaller and the gravity gradients in the $T_{r\lambda}$ direction do not reflect the terrain characteristics in detail.

1. Introduction

The gravity field and steady-state ocean circulation explorer (GOCE) gravity satellite was successfully launched by the European Space Agency in March 2009 [1,2] with a main task to measure Earth's gravity field and static current detection. GOCE is expected to provide a gravity model with an accuracy of 1 mGal for the gravity anomaly and 1 cm for the geoid. This satellite's mission will hopefully produce spherical harmonic coefficients of the Earth's gravity field to a degree and order of 300. It can measure gravity gradients through the perpendicular gravity gradiometer directly. We know that the gravity gradient is the second derivative of the gravitational potential. As a result, the gravity gradient is more sensitive to the distance. The GOCE gravity data set has been released since 2010; it includes original gravity gradient data in the Earth Fixed Reference Frame (EFRF) and the Local North Oriented Frame, precise science orbit data, and final gravity field model data. The data are always used to compute the regional gravity anomaly and

This work is supported by Key Projects of Henan Province Department of Education Science and Technology (14B420001).
* *Corresponding author.*
E-mail address: xhj0371@163.com (Xu H.).
Peer review under responsibility of Institute of Seismology, China Earthquake Administration.

Production and Hosting by Elsevier on behalf of KeAi

http://dx.doi.org/10.1016/j.geog.2015.01.001

geoid height; the use of these data is in a fledging period in geosciences research. Many scholars at home and abroad are conducting fruitful studies using simulative GOCE data. For example, Gruber [3] analyzed the validation of GOCE gravity field models; Knudsen [4] achieved a global mean dynamic topography and ocean circulation estimation using a GOCE gravity model; Bouman [5] researched the GOCE gravitational gradients along the orbit; Luo [6] and Li [7] studied the theory and method to recover Earth's gravity field; Wu [8,9] discussed the least squares collocation of harmonic analysis using the radial GOCE satellite gravity gradiometry (SGG) data; Wu [10] studied the method for preprocessing GOCE gravity gradient data in detail; Xu [11] discussed the accuracy evaluation method of GOCE SGG data based on satellite crossovers; Zhong [12,13] and Liu [14,15] researched the gridding method of the GOCE SGG data; Yang [16] acquired the gravity gradient tensor from gravity anomaly data. Nevertheless, studies on seismic activity using actual GOCE gravity field data are few. Zhang [17] studied the strong Ms9.0 earthquake in Japan and computed the gravity anomaly of the strong earthquake region with GOCE gravity field model data. Xu [18] obtained the gravity anomaly of mainland China using GOCE gravity field model data. Their result shows that the gravity anomaly computed from GOCE data is consistent with the tectonics of the earthquake region. Strong earthquakes usually occur in steep gravity gradient zones. As is known, the gravity gradient is the second derivative of the gravitational potential. As a result, it is more sensitive than the gravity anomaly. It is interesting to know whether the gravity gradients correlate with the tectonics distribution. Thus far, there have been no studies using actual GOCE measured gravity data to compute the entire gravity gradients for a specific region, to the best of our knowledge. In this study, the gravity gradient distribution in EFRF was obtained using actual measured GOCE gravity data.

2. Theoretical model and computing formula

The gravity anomaly has two definitions. One is the gravity value subtracted from the normal gravity value at the same point. In this case, it is also called the pure gravity anomaly. Another is the result after the gravity value on the geoid is subtracted from the normal gravity value on the corresponding reference ellipsoid; it is also called the mixed gravity anomaly. In this study, the mixed gravity anomaly was computed using GOCE data. The gravitational potential spherical harmonic series is given by Heiskanen/Moritz [19]:

$$\begin{aligned} V(r,\theta,\lambda) &= W(r,\theta,\lambda) - Q(r,\theta,\lambda) \\ &= \frac{GM}{r}\sum_{n=0}^{N_{\max}}\left(\frac{a}{r}\right)^{n}\sum_{m=0}^{n}(\overline{C}_{nm}\cos m\lambda + \overline{S}_{nm}\sin m\lambda)\overline{P}_{nm}(\cos\theta) \end{aligned} \tag{1}$$

where V is the gravitational potential at the computation point, W is the gravity potential, Q is the centrifugal potential, GM is the gravitational constant times total mass of the Earth (solid Earth, atmosphere, ocean). Furthermore, a is equatorial radius of the Earth ellipsoid used for the determination of the harmonic coefficients, n is degree of spherical harmonic series, $N_{\max}$ is maximum degree of spherical harmonic series, m is order of spherical harmonic series, r is radius distance of the computation point from the geocenter, θ is geocenter co-latitude of computation point, λ is geocentric longitude of computation point, $\overline{P}_{nm}$ represents normalized associated Legendre functions of degree n, and order m, $\overline{C}_{nm}$, $\overline{S}_{nm}$ are coefficients of the spherical harmonic series. After rescaling the spherical harmonic coefficients to the set of constants of the reference potential, the disturbing potential at a point P can be computed by

$$T_P = W_P - U_P \tag{2}$$

where W_P is gravity potential at point P (including centrifugal potential). U_P is normal potential of the reference ellipsoid at point P (including centrifugal potential), and T_P is the disturbing potential at point P.

If the gravity potential and normal gravity potential have the same centrifugal potential, the disturbing potential does not contain the effect of the centrifugal potential.

$$\begin{aligned} T_P(r,\theta,\lambda) &= W_P - U_P \\ &= \frac{GM}{r}\sum_{n=2}^{N_{\max}}\left(\frac{R}{r}\right)^{n}\sum_{m=0}^{n}(\Delta\overline{C}_{nm}\cos m\lambda \\ &\quad + \Delta\overline{S}_{nm}\sin m\lambda)\overline{P}_{nm}(\cos\theta) \\ &= \frac{GM}{R}\sum_{n=2}^{N_{\max}}\left(\frac{R}{r}\right)^{n+1}\sum_{m=0}^{n}(\Delta\overline{C}_{nm}\cos m\lambda \\ &\quad + \Delta\overline{S}_{nm}\sin m\lambda)\overline{P}_{nm}(\cos\theta) \end{aligned} \tag{3}$$

Formula (3) is the fundamental formula for the disturbing potential. Next we take a derivative to r, θ, λ. The results are as follows:

$$\begin{cases} T_r(P) = -\dfrac{GM}{R^2}\displaystyle\sum_{n=2}^{N_{\max}}\sum_{m=-n}^{n}(n+1)\left(\frac{R}{r}\right)^{n+2} t_{nm}Q_m(\lambda)\overline{P}_{n|m|}(\theta) \\ T_\theta(P) = \dfrac{GM}{R^2}\displaystyle\sum_{n=2}^{N_{\max}}\sum_{m=-n}^{n}\left(\frac{R}{r}\right)^{n+2} t_{nm}Q_m(\lambda)\frac{\partial\overline{P}_{n|m|}(\theta)}{\partial\theta} \\ T_\lambda(P) = \dfrac{GM}{R^2\sin\theta}\displaystyle\sum_{n=2}^{N_{\max}}\sum_{m=-n}^{n}\left(\frac{R}{r}\right)^{n+2} m t_{nm}Q_{-m}(\lambda)\overline{P}_{n|m|}(\theta) \end{cases} \tag{4}$$

The second partial derivatives are as follows:

$$\begin{cases} T_{rr}(P) = \dfrac{GM}{R^3}\displaystyle\sum_{n=2}^{N_{\max}}\sum_{m=-n}^{n}(n+1)(n+2)\left(\frac{R}{r}\right)^{n+3} t_{nm}Q_m(\lambda)\overline{P}_{n|m|}(\theta) \\ T_{\theta\theta}(P) = \dfrac{GM}{R^3}\displaystyle\sum_{n=2}^{N_{\max}}\sum_{m=-n}^{n}\left(\frac{R}{r}\right)^{n+3} t_{nm}Q_m(\lambda)\frac{\partial^2\overline{P}_{n|m|}(\theta)}{\partial\theta^2} \\ T_{\lambda\lambda}(P) = -\dfrac{GM}{R^3\sin^2\theta}\displaystyle\sum_{n=2}^{N_{\max}}\sum_{m=-n}^{n}\left(\frac{R}{r}\right)^{n+3} m^2 t_{nm}Q_m(\lambda)\overline{P}_{n|m|}(\theta) \\ T_{r\theta}(P) = -\dfrac{GM}{R^3}\displaystyle\sum_{n=2}^{N_{\max}}\sum_{m=-n}^{n}(n+1)\left(\frac{R}{r}\right)^{n+3} t_{nm}Q_m(\lambda)\frac{\partial\overline{P}_{n|m|}(\theta)}{\partial\theta} \\ T_{r\lambda}(P) = \dfrac{GM}{R^3\sin\theta}\displaystyle\sum_{n=2}^{N_{\max}}\sum_{m=-n}^{n}(n+1)\left(\frac{R}{r}\right)^{n+3} m t_{nm}Q_{-m}(\lambda)\overline{P}_{n|m|}(\theta) \\ T_{\theta\lambda}(P) = -\dfrac{GM}{R^3\sin\theta}\displaystyle\sum_{n=2}^{N_{\max}}\sum_{m=-n}^{n}\left(\frac{R}{r}\right)^{n+3} m t_{nm}Q_{-m}(\lambda)\frac{\partial\overline{P}_{n|m|}(\theta)}{\partial\theta} \end{cases} \tag{5}$$

Formula (5) refers to the first and second derivative of the Legendre function. The terms of $T_{\lambda\lambda}$, $T_{r\lambda}$, $T_{\theta\lambda}$ contain $1/\sin\theta$. In order to avoid the singular point during the computing process, i.e., in the south and north poles, $\sin(\theta) = 0$, a rigorous recursion formula was used in this study [20]. The specific calculation process is as follows:

$$\begin{cases} \dfrac{\partial \overline{P}_{n|m|}}{\partial \theta} = a^1_{nm}\overline{P}_{n,|m|-1} + a^2_{am}\overline{P}_{n,|m|+1} \\ a^1_{nm} = \dfrac{1}{2}\sqrt{n+|m|}\sqrt{n-|m|+1}\sqrt{\dfrac{2-\delta_{|m|0}}{2-\delta_{|m|-1,0}}} \\ a^2_{nm} = -\dfrac{1}{2}\sqrt{n-|m|}\sqrt{n+|m|+1}\sqrt{\dfrac{2-\delta_{|m|0}}{2-\delta_{|m|+1,0}}} \end{cases} \tag{6}$$

In formula (6) and henceforth, δ is the Kronecker sign function

$$\frac{\partial^2 \overline{P}_{n|m|}}{\partial \theta^2} = b^1_{nm}\overline{P}_{n,|m|-2} + b^2_{nm}\overline{P}_{n|m|} + b^3_{nm}\overline{P}_{n,|m|+2} \tag{7}$$

$$\begin{cases} b^1_{nm} = \dfrac{1}{4}\sqrt{n+|m|}\sqrt{n+|m|-1}\sqrt{n-|m|+1}\sqrt{n-|m|+2}\sqrt{\dfrac{2-\delta_{|m|0}}{2-\delta_{|m|-2,0}}} \\ b^2_{nm} = -\dfrac{1}{4}[(n+|m|)(n-|m|+1)+(n-|m|)(n+|m|+1)] \\ b^3_{nm} = \dfrac{1}{4}\sqrt{n+|m|+2}\sqrt{n+|m|+1}\sqrt{n-|m|}\sqrt{n-|m|-1}\sqrt{\dfrac{2-\delta_{|m|0}}{2-\delta_{|m|+2,0}}} \end{cases} \tag{8}$$

$$m\frac{\overline{P}_{n,|m|}}{\sin\theta} = c^1_{nm}\overline{P}_{n-1,|m|-1} + c^2_{nm}\overline{P}_{n-1,|m|+1} \tag{9}$$

$$\begin{cases} c^1_{nm} = \dfrac{m}{2|m|}\sqrt{n+|m|}\sqrt{n+|m|-1}\sqrt{\dfrac{(2-\delta_{|m|0})(2n+1)}{(2-\delta_{|m|-1,0})(2n-1)}} \\ c^2_{nm} = \dfrac{m}{2|m|}\sqrt{n-|m|}\sqrt{n-|m|-1}\sqrt{\dfrac{(2-\delta_{|m|0})(2n+1)}{(2-\delta_{|m|+1,0})(2n-1)}} \end{cases} \tag{10}$$

$$m^2\frac{\overline{P}_{n,|m|}}{\sin^2\theta} = d^1_{nm}\overline{P}_{n,|m|-2} + d^2_{nm}\overline{P}_{n,|m|} + d^3_{nm}\overline{P}_{n,|m|+2} \tag{11}$$

$$\begin{cases} d^1_{nm} = \dfrac{m^2}{4|m|(|m|-1)}\sqrt{\dfrac{2-\delta_{|m|0}}{2-\delta_{|m|-2,0}}} \\ \qquad \sqrt{n+|m|}\sqrt{n-|m|+1}\sqrt{n-|m|+2}\sqrt{n+|m|-1} \\ d^2_{nm} = \dfrac{m^2}{4|m|}\left[\dfrac{(n+|m|)(n+|m|-1)}{|m|-1} + \dfrac{(n-|m|)(n-|m|-1)}{|m|+1}\right] \\ d^3_{nm} = \dfrac{m^2}{4|m|(|m|+1)}\sqrt{\dfrac{2-\delta_{|m|0}}{2-\delta_{|m|+2,0}}} \\ \qquad \sqrt{n-|m|}\sqrt{n-|m|-1}\sqrt{n+|m|+2}\sqrt{n+|m|+1} \end{cases} \tag{12}$$

$$\frac{m}{\sin\theta}\frac{\partial \overline{P}_{n|m|}}{\partial\theta} = e^1_{nm}\overline{P}_{n-1,|m|-2} + e^2_{nm}\overline{P}_{n-1,|m|} + e^3_{nm}\overline{P}_{n-1,|m|+2} \tag{13}$$

$$\begin{cases} e^1_{nm} = \dfrac{m}{4(|m|-1)}\sqrt{\dfrac{(2-\delta_{|m|0})(2n+1)}{(2-\delta_{|m|-2,0})(2n-1)}} \\ \qquad \sqrt{n+|m|}\sqrt{n-|m|+1}\sqrt{n+|m|-1}\sqrt{n+|m|-2} \\ e^2_{nm} = \dfrac{m}{4}\left[\dfrac{\sqrt{n+|m|}(n-|m|+1)}{|m|-1} - \dfrac{(n+|m|+1)\sqrt{n+|m|}}{|m|+1}\right] \\ \qquad \sqrt{\dfrac{(2n+1)(n-|m|)}{2n-1}} \\ e^3_{nm} = -\dfrac{m}{4(|m|+1)}\sqrt{\dfrac{(2-\delta_{|m|0})(2n+1)}{(2-\delta_{|m|+2,0})(2n-1)}} \\ \qquad \sqrt{n-|m|}\sqrt{n+|m|+1}\sqrt{n-|m|-1}\sqrt{n-|m|-2} \end{cases} \tag{14}$$

We can obtain the gravity gradient distribution in a specific region through the above formulas.

3. The gravity gradient distribution in mainland China in EFRF

The study region is located at 70°–130° E and 15°–55° N. GOCE gravity field model data for the period Sep. 2009 to Jul. 2010 was used in this study. The order of the spherical harmonic coefficient was 250. The sample interval was $0.5° \times 0.5°$ and the average orbit altitude was 250 km. The terrain distribution in mainland China is shown in Fig. 1.

Fig. 1 shows the terrain of mainland China. The most famous mountain is the Qinghai-Tibet Plateau. There are many fault zones, such as the Altun fault, Kunlun fault, and Longmenshan fault.

Using the formulas (5–14), the gravity gradients of mainland China were computed in the $T_{\theta\theta}$, $T_{\lambda\lambda}$, T_{rr}, $T_{\vartheta\lambda}$, $T_{r\theta}$, $T_{r\lambda}$ directions respectively. The computing results are shown in Fig. 2(a)–(f).

The gravity gradient in mainland China was computed using GOCE gravity field model data for the first time. In Fig. 2, The results show that in the T_{rr} direction, the gravity gradients are the largest as compared with the other directions and the numerical value range is between $-3.5 \times 10^{-8}\ \mathrm{s}^{-2}$ and $+5.0 \times 10^{-8}\ \mathrm{s}^{-2}$. The data reflect the terrain characteristics in detail and correlate well with the tectonics. The gradient in the $T_{\theta\theta}$ and $T_{\lambda\lambda}$ directions reflect the terrain characteristics on the whole. However, the sign of the numerical value is opposite to that in the T_{rr} direction. The gradients of $T_{\theta\lambda}$ and $T_{r\lambda}$ are relatively small compared with the other directions and the numerical value range is between $-2.0 \times 10^{-8}\ \mathrm{s}^{-2}$ and $+2.0 \times 10^{-8}\ \mathrm{s}^{-2}$. In the $T_{r\theta}$ direction, the characteristics of the topography are revealed and they correlate well with the regional tectonics. In the $T_{r\lambda}$ direction, the gravity gradients do not reflect the terrain characteristics in detail.

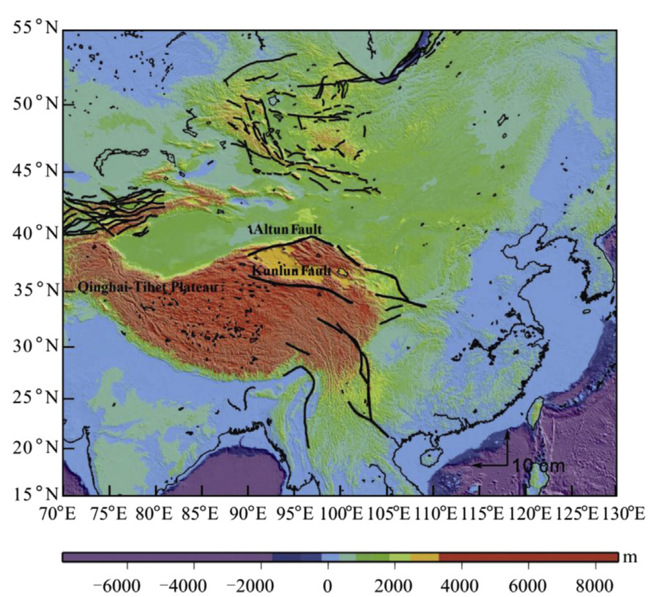

Fig. 1 – Terrain distribution in mainland China.

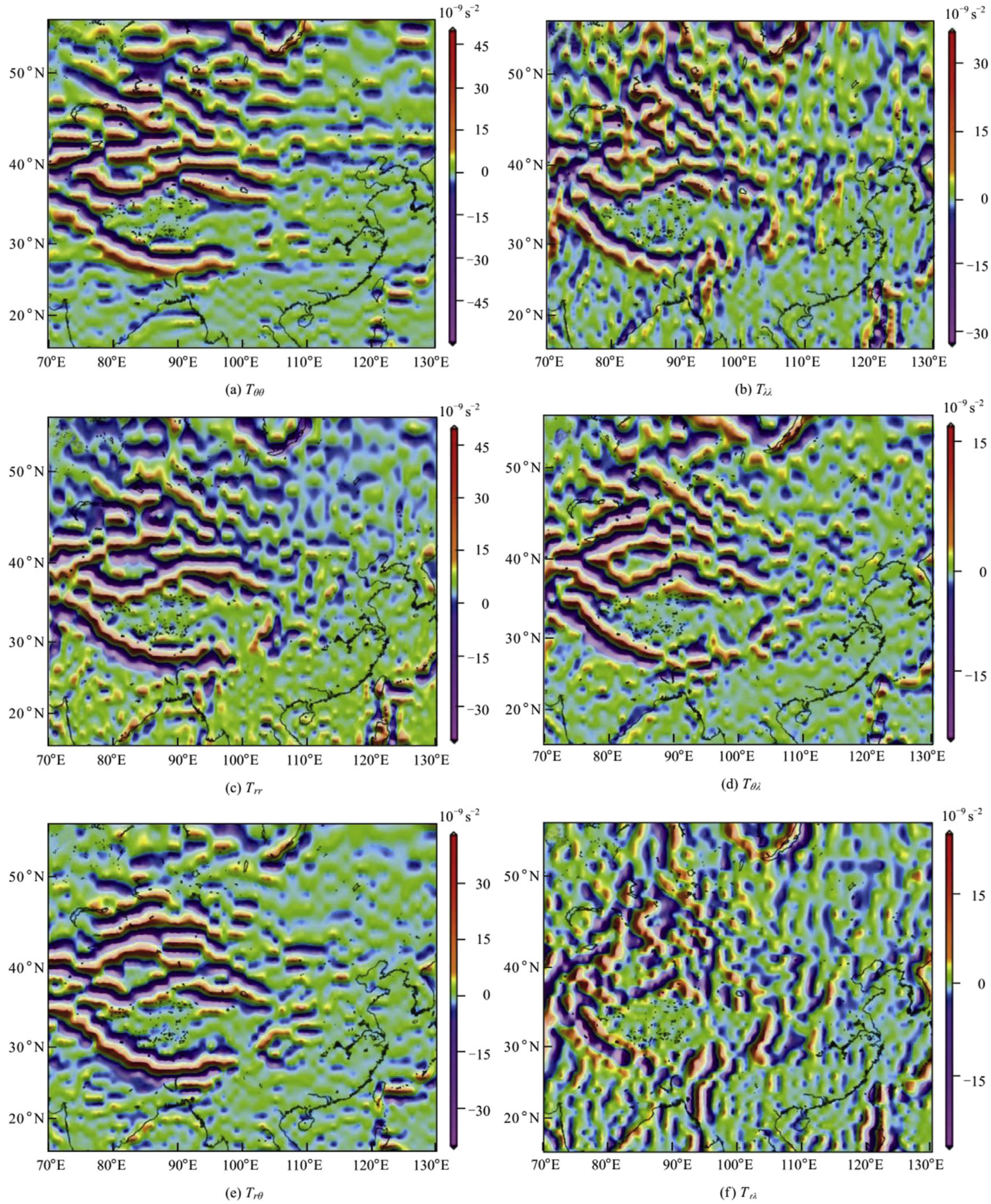

Fig. 2 — Gravity gradient distribution in EFRF Frame.

In summary, the gravity gradients computed using actual GOCE gravity field data correlate well with the geology at large scales, especially in the *Trr* direction. In the near future, higher resolution images using higher orders of GOCE gravity data will be obtained.

4. Conclusion

The results of this study show that the gravity gradients in the T_{rr} direction are the largest among all the six directions. Additionally, the gravity gradients in the T_{rr} direction correlate well with the terrain distribution in mainland China. The most probable reason for this may be that the gravity gradients in the *Trr* direction (also called the radial direction) are the nearest to the ground. As a result, the gravity gradients are more sensitive than those in the other directions.

Acknowledgments

The authors appreciate the European Space Agency for providing satellite gravity gradiometry data, and they are also very grateful to the anonymous reviewers for their advices to improve the explanation of the calculation results and the English writing. This paper was financially supported by Key Projects of Henan Province Department of Education Science and Technology (14B420001).

REFERENCES

[1] Drinkwater RM, Haagmans R, Muzi D. The GOCE gravity mission: ESA'a first core Earth explorer. In: Beutler GB, Drinkwater MR, Rummer R, Steiger Rvon, editors. Space science series of the ISSI, Earth gravity field from space-from sensors to Earth sciences. Dordrecht: Kluwer; 2007. p. 419–32.

[2] ESA. Gravity field and steady-state ocean circulation mission. ESA publication division special report. The Netherlands: ESTEC, Noordwijk; 1999. SP-1233(1).

[3] Gruber T, Visser PNAM, Ackermann C, Hosse M. Validation of GOCE gravity field models by means of orbit residuals and geoid comparisons. J Geod 2011;85:845–60.

[4] Knudsen P, Bingham R, Andersen O, Marie HR. A global mean dynamic topography and ocean circulation estimation using a preliminary GOCE gravity model. J Geod 2011; 85:861–79.

[5] Bouman J, Fiorot S, Fuchs M, Gruber T, Schrama E, Tscherning C, et al. GOCE gravitational gradients along the orbit. J Geod 2011;85:791–805.

[6] Luo Zhicai. Theory and method to determine earth's gravity field using satellite gravity gradiometry data. Wuhan: Wuhan Technical University of Surveying and Mapping; 1996 [in Chinese].

[7] Li Yingchun. Theory and method to recover earth's gravity field using satellite gravity gradiometry data. Zhengzhou: Information Engineering University of PLA; 2004 [in Chinese].

[8] Wu Xing. Theory and method to dispose the satellite gravity gradiometry data. Zhengzhou: Information Engineering University of PLA; 2009 [in Chinese].

[9] Wu Xing, Zhang Chuanding, Liu Xiaogang. Least-squares collocation harmonic analysis of the radial satellite gravity gradients. Acta Geoda etica Ca Rtogr Sinica 2010;39(5):471–7 [in Chinese].

[10] Wu Yunlong. Preprocessing study on GOCE satellite gravity gradiometry data. Wuhan: Wuhan University; 2010 [in Chinese].

[11] Xu Tianhe, He Kaifei. Accuracy evaluation method of GOCE SGG data based on satellite crossovers. Geomatics Inf Sci Wuhan Univ 2011;36(5):617–20 [in Chinese].

[12] Zhong Bo. Study on GOCE satellite gravimetry to determine earth's gravity field. Wuhan: Wuhan University; 2010 [in Chinese].

[13] Zhong Bo, Liu Hualiang, Luo Zhicai, Li Zhenhai. Reduction and gridded processing of satellite gravity gradient data. J Geodesy Geodyn 2011;31(3):79–84 [in Chinese].

[14] Liu Xiaogang, Wu Xiaoping, Wang Baojun. Meshing method study on satellite gravity gradiometry data. J Geodesy Geodyn 2010;30(6):60–5 [in Chinese].

[15] Liu Xiaogang, Wu Xiaoping, Zhao Dongming, Wu Xing. Comparison between trajectory disturbing gravity calculated with earth gravity field models of EGM96 and EGM2008. J Geodesy Geodyn 2009;29(5):62–7 [in Chinese].

[16] Yang Fang, Li Shanshan. Calculation and analysis of gradient tensors based on gravity anomaly information. Sci Surv Mapp 2011;36(1):65–6 [in Chinese].

[17] Zhang Yongzhi, Xu Haijun, Wang Weidong, Duan Hurong, Zhang Benping. Gravity anomaly from satellite gravity gradiometry data by GOCE in Japan Ms9.0 strong earthquake region. Procedia Environ Sci 2011;10:529–34.

[18] Xu Haijun, Zhang Yongzhi, Duan Hurong, Xia Chaolong. Gravity anomaly detected by GOCE satellite in China. Prog Geophys 2012;27(2):0404–8 [in Chinese].

[19] Heiskanen WA, Moritz H. Physical geodesy. San Francisco and London: W.H. Freeman and Company; 1967.

[20] Eshagh M. On satellite gravity gradiometry. Doctoral dissertation in Geodesy. Stockholm, Sweden: Royal Institute of Technology (KTH); 2009a.

Xu Haijun gained his doctor degree from Chang'an University in 2012 and his major is geodesy and survey engineering. His research area is satellite gravity survey, particle swarm algorithm inversion and the theory and application of three-dimensional laser scanner. He has published papers in domestic journals such as Journal of Geodesy and Geodynamics, Progress in Geophysics, Geophysical and Geochemical Exploration, Northwestern Seismological Journal, and so on. He works as a lecturer in North China University of Water Resources and Electric Power from July 2012.

He charge several scientific research projects, like Key Projects of Henan Province Department of Education Science and Technology (14B420001) and the Special Fund for Basic Scientific Research of Central Colleges (CHD2010ZY016).